Effect of valence subband dispersion on near-band-gap transitions in GaAs/$Al_xGa_{1-x}As$ quantum wells containing a two-dimensional electron gas

A. Gabbay, Yulia Preezant, E. Cohen, and B. M. Ashkinadze
Solid State Institute, Technion-Israel Institute of Technology, Haifa 32000, Israel

L. N. Pfeiffer
Bell Laboratories, Alcatel-Lucent Technologies, Murray Hill, New Jersey 07974, USA

(Received 26 December 2007; published 21 April 2008)

The reflection (R) and photoluminescence (PL) spectra of several GaAs/$Al_xGa_{1-x}As$ modulation-doped quantum wells (MDQWs) were studied at $T=2$ K. The n doping was either on one side of the quantun well (width of 25 nm) or symmetrically on both sides (width of 20 nm), and the resulting two-dimensional electron gas (2DEG) density was in the range of $n_e=(0.7-2.0)\times10^{11}$ cm^{-2}. The reflection spectra of the two-side MDQW's show sharp but weak lines ($\Delta R<0.02$), which are attributed to e1-hh1 and e1-lh1 interband transitions at in-plane wave vectors $k_{\|}=k_F$. These spectra were analyzed by calculating the dispersion of the lowest conduction and top valence subbands and the contribution of the 2DEG interband transitions to the MDQW optical susceptibility. The reflection spectral shape was then calculated as a function of n_e and of the layer widths. This model explains the observed differences between the intensity and line shape of the one-side and two-side MDQW's. The PL spectral shape of all the MDQW's shows a marked dependence on laser excitation intensity. It was calculated by using the e1 and hh1 dispersion curves and assuming that the interband transitions are $k_{\|}$ conserving. The observed PL spectral dependence on laser excitation intensity was analyzed by assuming that the effective temperature of the photoexcited holes increases with excitation intensity in the range of $T_h=4-15$ K, while the 2DEG temperature remains unchanged and equal to that of the lattice.

DOI: 10.1103/PhysRevB.77.165329 PACS number(s): 73.21.Fg, 78.67.De

I. INTRODUCTION

Interband spectroscopy of semiconducting modulation-doped quantum wells (MDQW's) is used to study the electronic properties of the two-dimensional gas of majority carriers in the presence of photoexcited minority carriers.[1,2] The nature of interband transitions in n-MDQW's depends on the two-dimensional electron gas (2DEG) density. Neutral and negatively charged exciton lines dominate the interband spectra at low densities, while no bound electron-hole (e-h) pair states exist at high densities, and the spectra are due to holes that are weakly interacting with the entire 2DEG.[3–5] In the latter case, the photoluminescence (PL) spectrum is characterized by a broad band that extends over the energy range $E_G'<E<E_F$, where E_G' is the renormalized band-gap energy and E_F is the Fermi energy.[6] No absorption or PL excitation (PLE) occurs in this energy range. The transition between excitonic spectra and 2DEG-free hole spectra was observed in GaAs/$Al_xGa_{1-x}As$ n-MDQW's with 2DEG density in the range of $n_e\sim0.5\times10^{11}$ cm^{-2}. The density at which this transition occurs depends on sample quality and on the method by which n_e is varied.[7–9]

A pronounced intensity enhancement is often observed in the PL and PLE spectra near E_F at low temperatures.[10–12] This Fermi edge singularity (FES) arises from electron–photoexcited hole scattering into unoccupied states having in-plane wave vectors $k_{\|}>k_F$.[13–16] The FES intensity was found to depend on several factors: (1) it increases with increasing hole localization.[17–19] The degree of in-plane hole localization is determined by the quantum well (QW) interface quality and by alloy fluctuations in the QW material.[20] (2) The proximity of an unoccupied, higher energy electron subband to E_F. When the 2DEG occupies only the lowest conduction subband (e1), the FES is enhanced by the admixture of (e1-hh1) (k_F) pair excitations with exciton states that are formed of the next subbands, namely, (e2-hh2).[11,12,21,22] Recently, circularly polarized absorption spectra of n-MDQW's with n_e in the range of $(0.4-2.4)\times10^{11}$ cm^{-2} were studied under a perpendicularly applied magnetic field and at ultralow temperatures.[23] The observed FES was interpreted as due to a Mahan exciton[13] when the spin polarization is parallel to that of the 2DEG motional polarization and to a power law enhancement in the antiparallel case.[14]

The availability of GaAs/$Al_xGa_{1-x}As$ n-MDQW's having a 2DEG with very high mobility[24] allows the study of interband transitions that are virtually unaffected by electron and hole localizations. It was demonstrated that in such structures, the 2DEG density above which no excitons are formed can be very low (around $n_e\sim0.5\times10^{10}$ cm^{-2}).[25,26] In the present work, we studied the reflection and PL spectra near E_G' of several δ-doped GaAs/$Al_xGa_{1-x}As$ QW's with various 2DEG densities. All of the studied n-MDQW's have a very high mobility [in the range of $\mu_e=(2-7)\times10^6$ cm^2/V s at $T=2$ K]. They show narrow reflection features at E_F and a broad PL spectrum in the range $E_G'<E<E_F$, with its peak intensity just above E_G'. Reflection spectroscopy was preferred in this study over PLE or absorption spectroscopy because the PLE involves intervening hole relaxation processes, while absorption requires etching off the GaAs substrate, and this results in strained samples. The main objective of this paper is to analyze the interband transitions that are observed in n-MDQW's where the effects of hole localization are negligible and the interband transitions at k_F are not admixed with excitons formed of higher energy transi-

tions. The analysis of the energy and band shape of the observed interband transitions was done in three stages: (1) calculating the dispersion of the lowest conduction subband (e1) and of the top valence subbands (hh1 and lh1), including the 2DEG potential (in the Hartree approximation[4,27]); (2) calculating the energy-dependent optical susceptibility function for the interband transitions in the (e1-hh1) and (e1-lh1) spectral range[28] (this function was then used for the MDQW refraction index in the calculation of the reflection spectra by the method of transfer matrices);[29] and (3) calculating the PL spectral shape by using the dispersion curves and assuming $k_{\|}$-conserving interband transitions.[30]

The paper is laid out as follows: Sec. II details the structure of the MDQW samples under study and their 2DEG parameters. It also details the experimental procedures and presents representative reflection and PL spectra. Section III explains the assumptions underlying the models and the calculation methods. Section IV describes the model fitting of the observed spectra. Section V is a summary that lists the conclusions drawn from the model fittings, pointing out the particular properties of intrinsic interband transitions (namely, those observed in *n*-MDQW's having a high mobility 2DEG).

II. EXPERIMENTAL DETAILS AND REPRESENTATIVE REFLECTION AND PHOTOLUMINESCENCE SPECTRA

The MDQW GaAs/$Al_xGa_{1-x}As$ structures studied here were grown by molecular beam epitaxy on (001)-oriented GaAs wafers. They were of two types: (1) MDQW's that are δ-doped on one side of a 25-nm-wide QW (one-side MDQW's). Their layer sequence consists of a wide GaAs buffer layer, a 100-period GaAs/$Al_{0.3}Ga_{0.7}As$ superlattice, the 25-nm-wide GaAs QW, a wide $Al_{0.3}Ga_{0.7}As$ layer that contains a δ-doped Si layer, and a GaAs cap layer.[31] (2) MDQW's that have two wide $Al_{0.1}Ga_{0.9}As$ layers, which contain δ-doped Si layers that were grown symmetrically on both sides of a 20-nm-wide GaAs QW. The width of the $Al_xGa_{1-x}As$ spacer layers separating each one of the δ-doped layers from the QW varied in the range of 50–100 nm, depending on the doping level. The 2DEG density range is $n_e=(0.7-2.0)\times10^{11}$ cm^{-2}. These MDQW's are considered to be of high quality since their measured Hall mobility is in the range of $\mu_e=(2-7)\times10^6$ cm^2/V s (at $T=2$ K).[31,32] A schematic representation of the two MDQW types studied here is shown in the insets of Figs. 1(b) and 1(d). An undoped GaAs/$Al_{0.18}Ga_{0.82}As$ multiple QW structure was also studied for a comparison with the MDQW spectra.

Reflection and PL spectra were measured with the sample immersed in liquid He at $T=2$ K. It was illuminated with a tungsten filament lamp for reflection measurements and with a Ti:sapphire laser for PL excitation. The exciting laser energy E_L was set below the band gap energy of the AlGaAs barrier (in order to avoid optical depletion) and the laser intensity was varied (but kept low, $I_L\leq0.25$ W/cm^2). The reflection and PL spectra were detected and spectrally analyzed with a double-grating spectrometer (having a resolution of 0.03 meV) equipped with a cooled charge coupled device camera.

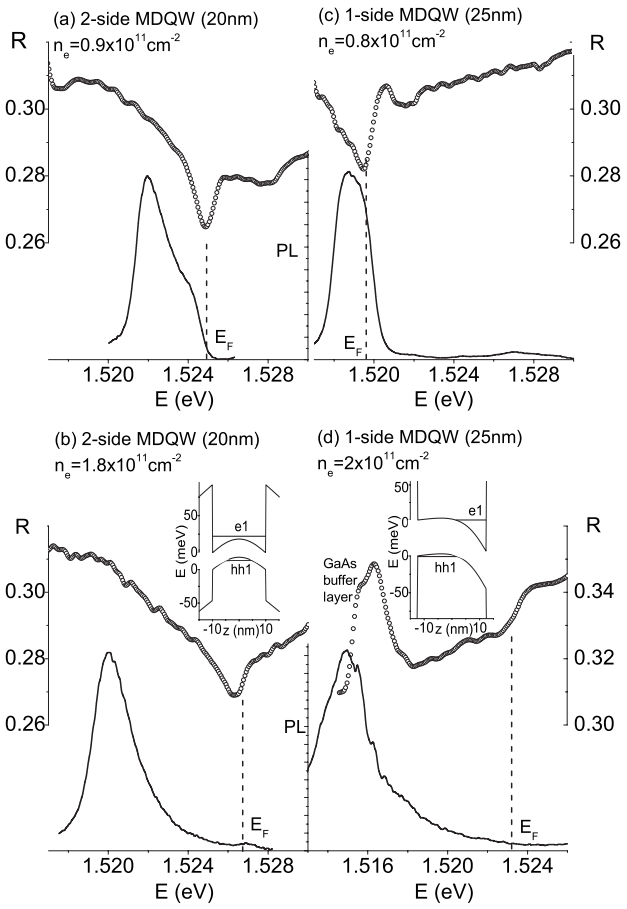

FIG. 1. [(a)–(d)] Reflection (circles) and PL (solid lines) spectra of several one-side and two-side MDQW's measured at $T=2$ K. The reflection scale (shown in each figure) was determined by normalizing the measured spectrum with respect to the reflection of a distributed Bragg reflector (that is, $R\sim1$ in the studied spectral range). Note that in the reflection spectrum of (d), only the feature at E_F is due to the presence of a 2DEG. A schematic representation of the two MDQW structures is shown in (b) and (d) by the energy dependence of the conduction and valence band edges on z (the growth direction coordinate). The energies of the lowest conduction and top valence subbands are also shown.

Figure 1 shows the reflection and PL spectra of several MDQW's. The reflection scale of all spectra was determined by normalizing the measured spectrum with respect to the reflection of a distributed Bragg reflector (that is virtually totally reflecting in the studied spectral range). Figure 2 shows two series of PL spectra of the two-side MDQW's with $n_e=0.9\times10^{11}$ and 2.0×10^{11} cm^{-2}, which were measured with increasing laser excitation intensity I_L. It is noted that no enhancement is observed at E_F in all of the PL spectra (Figs. 1 and 2), except for a slight intensity increase in Fig. 1(b). The spectra shown in Figs. 1 and 2 are representative of those measured for all other MDQW's (see Sec. IV).

III. MODEL

The models used for the interpretation of the observed reflection and PL spectra are based on the following assump-

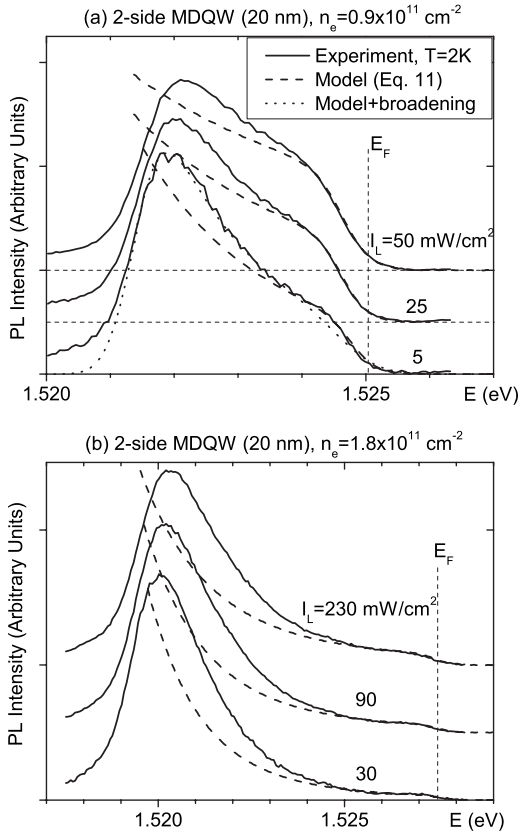

FIG. 2. PL spectra (solid lines) of the two two-side MDQW's measured at an ambient temperature of $T=2$ K. The PL was excited with a laser energy of $E_L=1.58$ eV and with varying intensity as indicated in the figures. Each spectrum was normalized with respect to its integrated intensity. The dashed lines are the spectra calculated by using the model explained in Sec. III. The dotted curve shown at the bottom spectrum of (a) was calculated by convoluting the distribution functions of Eq. (11) with a Gaussian broadening function (width $\Delta E=0.8$ meV, $T_h=5$ K).

tions: (1) the energies of the electrons and holes involved in the interband transitions are those of noninteracting particles. The 2DEG effect on the energies is through the averaged Coulomb potential, $\Phi(z)$, calculated in the Hartree approximation.[27] This potential is then incorporated into the Hamiltonians of both electrons and holes.[4] (2) The reflection spectrum over a wide range of energies above E_F is determined by vertical interband transitions involving unoccupied electron states. Their energy is calculated from the conduction and valence subband dispersion curves and their transition dipole is approximately independent of $k_{\|}$.[28] (3) The weak electron-hole interaction effect is discerned only near the Fermi edge. This effect is simulated by an enhanced strength of the interband transition dipole in the range of $k_{\|}\sim k_F$. (4) The PL spectrum in the energy range $E'_G<E<E_F$ is approximately determined by a Boltzmann distribution of holes within the valence subbands, which is described by an effective hole temperature.

We begin by calculating the dispersion of the conduction and valence subbands as a function of the 2DEG density. For the conduction band, the effect of the MDQW confining potential energy $V_C(z)$ and of the Hartree potential energy $(-e)\Phi(z)$ can be separated from the in-plane electron motion. Then, the z-dependent Schrödinger equation is

$$\left[-\frac{\hbar^2}{2}\frac{\partial}{\partial z}\frac{1}{m_c^*(z)}\frac{\partial}{\partial z}+V_c(z)-e\Phi(z)\right]\psi(z)=E\psi(z). \quad (1)$$

It is solved simultaneously with the one-dimensional Poisson equation in a self-consistent way. The first term is the kinetic energy, with a position-dependent conduction band effective mass $m_c^*(z)$. The 2DEG charge distribution in the QW is given by $-(e)n_e|\psi_{e1}(z)|^2$ (except for the initial iteration, when it is assumed to be uniformly distributed within the MDQW.) In all of the MDQW's studied here, and at $T=2$ K, the 2DEG occupies only the lowest conduction subband (e1), so that the 2DEG charge distribution is determined only by the z-dependent part of the e1 subband wave function $\psi_{e1}(z)$. The in-plane dispersion $E_{e1}(\mathbf{k}_{\|})$ is taken to be parabolic, and it is computed with the electron effective masses of bulk GaAs and bulk $Al_xGa_{1-x}As$ in the well and in the barriers, respectively.[33]

The valence subbands that are derived from the top Γ_8 band are obtained using the following Hamiltonian:

$$H_v=T_v+V_v(z)-e\Phi(z). \quad (2)$$

The hole in-plane motion and its motion along z are admixed by the kinetic energy term T_v, which is given by the 4×4 Luttinger matrix[34,35] (in electron representation)

$$T_v=\begin{pmatrix} P+Q & S & R & 0 \\ S^* & P-Q & 0 & R \\ R^* & 0 & P-Q & -S \\ 0 & R^* & -S^* & P+Q \end{pmatrix}, \quad (3)$$

$$P=-\frac{\hbar^2}{2m_0}\gamma_1(z)k^2, \quad (4)$$

$$Q=-\frac{\hbar^2}{2m_0}\gamma_2(z)(k_x^2+k_y^2-2k_z^2), \quad (5)$$

$$S=\frac{\hbar^2}{m_0}\sqrt{3}\gamma_3(z)k_z(k_x-ik_y), \quad (6)$$

$$R=\frac{\hbar^2}{2m_0}\sqrt{3}\gamma_2(z)(k_x^2-k_y^2)-i\frac{\hbar^2}{m_0}\sqrt{3}\gamma_3(z)k_xk_y. \quad (7)$$

Here, $\gamma_1(z)$, $\gamma_2(z)$, and $\gamma_3(z)$ are the position-dependent Luttinger parameters. At the interface between the QW and its barrier, the values of the Luttinger parameters are taken as the average of those of GaAs and $Al_xGa_{1-x}As$ layer materials. The Schrödinger equation is then numerically solved. For the present study, the calculated $E_{hh1}(\mathbf{k}_{\|})$ and $E_{lh1}(\mathbf{k}_{\|})$ dispersions and the corresponding wave functions are needed.

Once the subband energies and wave functions are obtained as a function of $k_{\|}$, the contribution of the MDQW interband transitions to the optical susceptibility function is calculated[28] as follows:

$$\chi_e(E) = \sum_{\mathbf{k}_\parallel, i} \frac{|d_{e1,hi}(\mathbf{k}_\parallel)|^2}{S_{QW} L_{QW}} [f_c(E_{e1}(\mathbf{k}_\parallel)) - f_v(E_{hi}(\mathbf{k}_\parallel))] \times \left[\frac{1}{[E_{hi}(\mathbf{k}_\parallel) - E_{e1}(\mathbf{k}_\parallel) + E + i\gamma(\mathbf{k}_\parallel)]} - \frac{1}{[E_{e1}(\mathbf{k}_\parallel) - E_{hi}(\mathbf{k}_\parallel) + E + i\gamma(\mathbf{k}_\parallel)]} \right]. \quad (8)$$

When the interband transitions are studied over a wide spectral range, the transition dipoles $d_{e1,hi}$ (hi=hh1,lh1) are frequently assumed to be $k_\parallel$ independent.[28] However, in the present case, the model must account for the sharp reflection lines that appear near E_F. This requires adding to $d_{e1,hi}$ an enhancement term that originates in the e-h interaction near k_F:

$$d_{e1,hi}(k_\parallel) = a_i + b_i \exp\left\{ - \frac{\frac{\hbar^2}{2m_c^*}(k_\parallel - k_F)^2}{\sigma_1^2} \right\}. \quad (9)$$

The photoexcited electron-hole pair dephasing is due to scattering into unoccupied states with $k_\parallel > k_F$, and it is taken as

$$\gamma(k_\parallel) = \gamma_0 \left(1 - \exp\left\{ - \frac{\frac{\hbar^2}{2m_c^*}(k_\parallel - k_F)^2}{\sigma_2^2} \right\} \right) \Theta(k_\parallel - k_F) + \gamma_{min}. \quad (10)$$

Here, $\Theta(x)$ is the step function. γ_{min} is a fixed rate that represents scattering of the e-h pair with electrons deep in the Fermi sea. The term containing the Gaussian function describes an enhanced dephasing rate for scattering involving electrons above k_F.[13,14]

The total MDQW optical susceptibility function is given by $\chi = \chi_{GaAs} + \chi_e$. From it, the refraction index of the MDQW layer is calculated: $n(E) = \mathrm{Re}(n) + \mathrm{Im}(n) = (1 + 4\pi\chi)^{1/2}$. Fixed refractive indices are used for each constituent layer. The reflection spectrum of the entire structure under study is then calculated by using the transfer matrix method.[29]

Finally, the low temperature PL spectral shape is interpreted by a model that describes the hole distribution along the dispersion curve of the hh1 valence subband, in the range $k_\parallel < k_F$. In high mobility MDQW's, such as those studied here, both electrons and holes are considered free and, thus, only vertical transitions are considered ($k_{\parallel e} = k_{\parallel h}$). The transition dipole moment $d_{e1,hh1}$ is assumed to be independent of $k_\parallel$ in the entire range $0 < k_\parallel < k_F$ with no enhancement at E_F. The PL intensity as a function of photon energy $\hbar\omega = E_{e\text{-}h}(k_\parallel) = E_{e1}(k_\parallel) - E_{hh1}(k_\parallel)$ is given by[30]

$$I(\hbar\omega) \propto \sum_{\mathbf{k}_\parallel} f_{e1,k_\parallel}(1 - f_{hh1,k_\parallel}) \delta[\omega - \omega_{e1,hh1}(k_\parallel)]. \quad (11)$$

$f_{c,k_\parallel}$ is the Fermi–Dirac distribution function of the 2DEG and $f_{v,k_\parallel}$ is the Boltzmann distribution function of the photoexcited holes. Both electron and hole distribution functions are assumed to depend on effective temperatures (T_e and T_h, respectively).[36] However, under the low photoexcitation intensities used in the present study, the 2DEG is assumed to remain at equilibrium with T_e slightly higher than the lattice temperature. The underlying assumption for the photoexcited holes is that they are heated by phonons emitted by the 2DEG during the 2DEG-free hole radiative lifetime, and this results in a Boltzmann distribution with $T_h > T$.[37]

IV. MODEL FITTING OF THE REFLECTION AND PHOTOLUMINESCENCE SPECTRA

A. Luttinger parameters of the modulation-doped quantum wells

In order to study the effect of the 2DEG potential on the dispersion of the conduction and valence subbands, the Poisson and Schrödinger equations are solved simultaneously, in a self-consistent way, for electrons occupying the e1 subband at $T=0$. Then, the resulting Hartree potential energy $(-e)\Phi(z)$ is introduced into the valence band Hamiltonian. Before doing it, the Luttinger parameters γ_i, $i=1-3$, that define the hole kinetic energy [Eqs. (3)–(7)] are required. Various sets of Luttinger parameters of $GaAs/Al_xGa_{1-x}As$ QW's were reported in the studies of interband transitions,[38,39] intersubband absorption,[40] and Raman scattering.[41] In many studies of PLE and absorption spectroscopy, the energies of excitons associated with the e2-hh2 and e2-lh2 transitions are determined.[42] From these, the electron and hole confinement energies, namely, the energies of the conduction and valence subbands at $k_\parallel = 0$, were obtained by using the exciton binding energies.[3,43] However, these energies are determined only by γ_1 and γ_2.[44] In the present study of MDQW's, the observed interband transitions involve unbound e-h pairs. Their energies can be compared with those of the (e1-hh1)2S and (e1-lh1)2S excitonic transitions in undoped QW's. The reason for this is the small binding energies ($\sim$1 meV) of the 2S excitons.[43]

We therefore compare the reflection spectrum of an undoped, 20-nm-wide $Al_{0.18}Ga_{0.82}As$ QW [Fig 3(a)] with the spectra of the two two-side MDQW's [Figs 3(b) and 3(c)]. The undoped QW shows sharp lines that are due to the 1S and 2S excitons associated with the (e1-hh1) and (e1-lh1) transitions. The energies of the e1, hh1, and lh1 confined states are calculated by using the following parameter values: $\gamma_1 = 6.9$ and $\gamma_2 = 1.85$. By adding to them the GaAs band-gap energy, the energies of the (e1-hh1) and (e1-lh1) transitions at $k_\parallel = 0$ are obtained (shown by vertical arrows). They fit the measured energies of the (e1:hh1)2S and (e1:lh1)2S excitons as well as that of the (e2:hh2)2S exciton (not shown). The γ_1 and γ_2 parameter values used here agree well with those reported in Refs. 41 and 43. By referring now to the case of MDQW's, interband transitions appear in reflection and absorption spectra only for $E_{e\text{-}h}(k_\parallel > k_F)$ and in the PL spectrum only for $E_{e\text{-}h}(0 < k_\parallel < k_F)$. We therefore identify the sharp lines in the reflection spectra of the MDQW's [near E_F, Figs. 1(a)–1(d)] as e-h transitions at $k_\parallel = k_F$. These transitions are also indicated (by vertical arrows) in Figs. 3(b) and 3(c) and we use their energy in order to extract γ_3. As the Luttinger matrix shows, the value of γ_3 can be determined only when hole states with $k_\parallel > 0$ are involved. We thus calculated the dispersion curves of the top valence

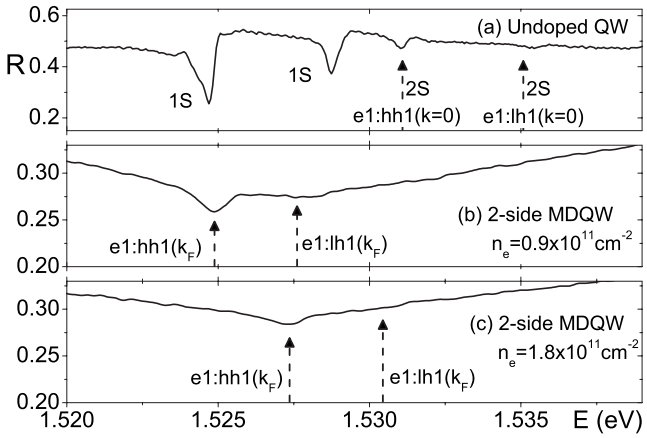

FIG. 3. Reflection spectra measured at $T=2$ K: (a) an undoped $Al_{0.18}Ga_{0.82}As$ QW. The calculated energies of the (e1-hh1) and (e1-lh1) transitions at $k_{\|}=0$ are indicated by vertical arrows. They coincide with the sharp lines that are usually identified as (e1:hh1)2S and (e1:lh1)2S excitonic transitions, respectively. [(b) and (c)] Two-side MDQW's with indicated 2DEG densities. The vertical arrows show the calculated energies of the (e1-hh1) and (e1-lh1) transitions at k_F.

subbands by using the Hamiltonian of Eq. (2) with the value of $\gamma_3=2.9$.[33] Figure 4 shows the dispersion curves calculated for the 20-nm-wide, two-side MDQW with $n_e=1.8\times10^{11}$ cm^{-2}. The in-plane anisotropy of the valence subbands is demonstrated by showing the dispersion curves along the (010) and (110) directions (solid and dashed lines, respectively). However, in order to compare the measured interband transition energies with the calculated ones, the renormalized band-gap energy E_g' is required. It is obtained

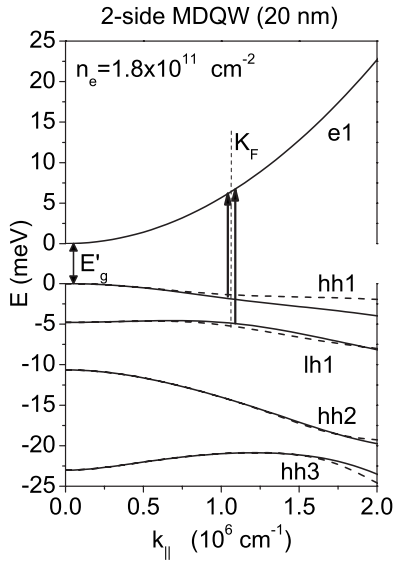

FIG. 4. Dispersion curves of the lowest conduction subband (e1) and top four valence subbands (hh1, lh1, hh2, and hh3), which are calculated in the Hartree approximation for the 20-nm-wide, two-side MDQW with $n_e=1.8\times10^{11}$ cm^{-2}. The in-plane anisotropy of the valence subbands is demonstrated by showing the dispersion curves along the (010) and (110) directions (solid and dashed lines, respectively).

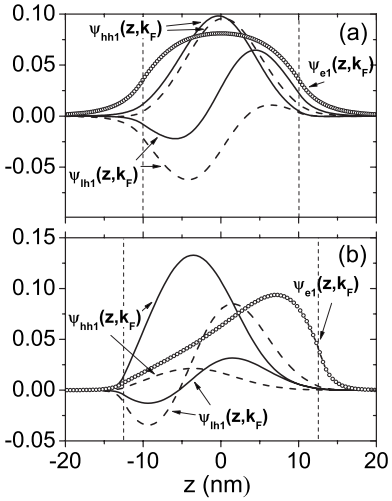

FIG. 5. The calculated dependence of the wave functions $\psi_{e1}(z,k_F)$, $\psi_{hh1}(z,k_F)$, and $\psi_{lh1}(z,k_F)$ on z (along the confinement direction) for two MDQW's: (a) symmetrically doped on two sides, $n_e=1.8\times10^{11}$ cm^{-2}. (b) One-side doped, $n_e=2.0\times10^{11}$ cm^{-2}. Circles, real wave function of e1; solid and dashed lines, real and imaginary parts of the hh1 and lh1 wave functions, respectively; thin vertical lines, QW boundaries.

from the fitted PL spectra (Fig 2) with an accuracy of 1 meV. The diagonalization of the valence band Hamiltonian yields the hole wave function for each subband. As an example, we show in Figs 5(a) and 5(b) the wave functions $\psi_{e1}(z,k_F)$, $\psi_{hh1}(z,k_F)$, and $\psi_{lh1}(z,k_F)$, which are calculated along the confinement direction z for the two types of MDQW's studied here. These were calculated at k_F since their overlap integrals are needed for the analysis of the reflection lines, which are observed at E_F. As these plots show, there are differences between the wave functions of the MDQW that is symmetrically doped on two sides and the asymmetrically doped MDQW.

B. Optical susceptibility and reflection spectrum

The optical susceptibility that is due to near-band-gap interband transitions of the MDQW containing a 2DEG in the QW is now calculated by using Eqs. (8)–(10) and with the calculated dispersion curves of the e1, hh1, and lh1 subbands. By using it, the refraction index function is calculated. Examples are shown in Fig. 6(a) for the two-side MDQW's with $n_e=0.9\times10^{11}$ cm^2 and $n_e=1.8\times10^{11}$ cm^{-2}. They were calculated with the values of a_i and b_i, which are given in Table I. The reflection spectrum was calculated for each one of the studied MDQW structures by using the transfer matrix method. In order to demonstrate the 2DEG effect on the reflection spectrum, it was calculated for the two-side MDQW structure, which has 2DEG with $n_e=0.9\times10^{11}$ cm^{-2}, in two cases: (a) the transition dipoles of the 2DEG interband transitions are taken to be independent of $k_{\|}$ [namely, $b_i=0$ in Eq. (9)]; (b) the transition dipoles of the 2DEG interband transitions include the enhancement terms as given in Eq. (9) ($b_i>0$). In Fig. 6(b), the results clearly demonstrate that the 2DEG enhancement terms are

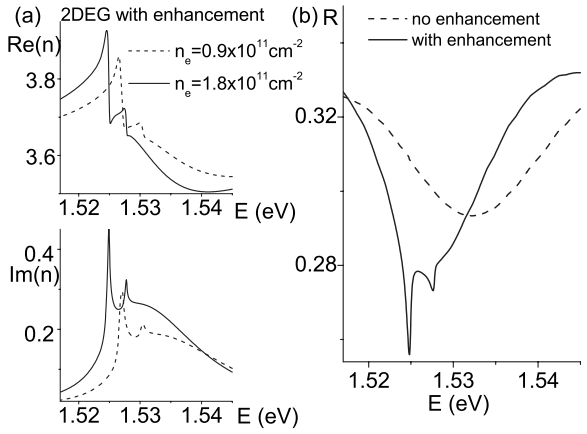

FIG. 6. (a) The refraction index function calculated for two two-side MDQW's with the indicated n_e. (b) Calculated reflection spectra for a two-side MDQW with $n_e=0.9\times10^{11}$ cm^{-2}. Dashed line, transition dipoles of the 2DEG interband transitions that are independent of $k_\parallel$ [namely, $b_i=0$ in Eq. (9)]; solid line, transition dipoles containing an enhancement near k_F as described in Eq. (9). The values of a_i and b_i are given in Table I.

essential to produce sharp lines at the Fermi edge. The measured reflection spectra of the MDQW structures that exhibit sharp features near k_F were fitted with the optical susceptibility function that was calculated with the parameter values given in Table I. We chose to show the values of a_i^2 and b_i^2 (given in meV) because they allow a meaningful comparison of the 2DEG transition dipole (squared) with the value of $E_p=2E_G^2m_0d_{cv}^2/(\hbar e)^2$ (=22 eV for GaAs).[45] This is the energy associated with the conduction-valence interband transition dipole, d_{cv}^2. Similarly, the values of the Gaussian broadening parameters σ_i^2 are given in meV because they can then be compared with the values of E_F. The quality of the model fitting to the measured reflection spectra is examined as follows. It is known[28,46] that the reflection spectrum of a given layer structure depends on each layer width and on the refraction index of the layer material. We measured the reflection spectrum of the two two-side MDQW structures at several points on the sample surface, which are spaced ~3 mm apart. The layer widths in these structures were measured to increase from point to point by ~1.3% for every 1 mm. By using this variation and the same 2DEG optical susceptibility function, the reflection spectrum was calculated for the two points of measurements and the results are shown in Fig. 7. The agreement of the calculations with the measured spectra demonstrates the accuracy of the optical susceptibility model.

TABLE I. Optical susceptibility model parameters for two-side MDQW's. All values are in meV.

n_e	0.9×10^{11} cm^{-2}	1.8×10^{11} cm^{-2}
$(a_{e1\text{-}hh1})^2$	31	19
$(a_{e1\text{-}lh1})^2$	6.9	3.5
$(b_{e1\text{-}hh1})^2$	6200	3800
$b_{(e1\text{-}lh1)^2}$	1400	600
$(\sigma_{1,e1\text{-}hh1})^2$	9.7	15.3
$(\sigma_{1,e1\text{-}lh1})^2$	8.6	14.6
$\gamma_{0,e1\text{-}hh1}$	5	5
$\gamma_{0,e1\text{-}lh1}$	5	5
$\gamma_{min,e1\text{-}hh1}$	0.05	0.05
$\gamma_{min,e1\text{-}lh1}$	0.05	0.05
$(\sigma_{2,e1\text{-}hh1})^2$	1.1	1.8
$(\sigma_{2,e1\text{-}lh1})^2$	0.9	1.2

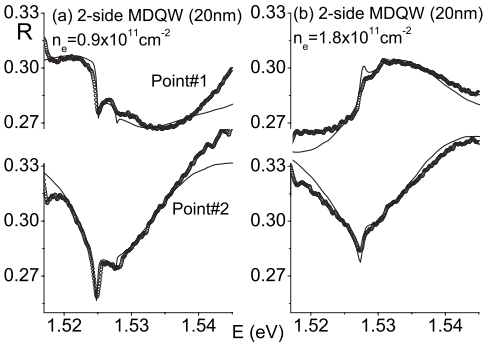

FIG. 7. Reflection spectra measured at two points on the sample surface that are separated by 3 mm (circles). The calculated spectra (solid lines) use the same optical susceptibility function as for the 2DEG layer. The layer widths between the two measured points differ by 4%. (a) Two-side MDQW with $n_e=0.9\times10^{11}$ cm^{-2}. (b) Two-side MDQW with $n_e=1.8\times10^{11}$ cm^{-2}.

The underlying physical mechanism that causes the appearance of Fermi edge enhancement in PL spectra is 2DEG-photexcited hole scattering.[13–16] It has been shown that this enhancement increases with hole localization[17–19] and when the e-h pair transitions near k_F interact resonantly with an exciton that is associated with transitions between higher energy subbands.[11,12,21,22] In the MDQW studied here, neither situation exists, and the observed reflection intensity of the sharp lines at k_F is very small: $\Delta R<0.02$. We thus conclude that the Fermi edge enhancement is due to 2DEG-free hole scattering near k_F. The transition dipole functional dependence on $k_\parallel$ [Eq. (9)] is chosen to model the Fermi edge enhancement. Support for this choice is derived from examining the calculated overlap integral of the electron and hole wave functions at k_F, $S_{e1\text{-}hi}$, for e1 and hi=hh1, 1h1 as follows:

$$S_{e1\text{-}hi}=\left|\int \Psi_{hi}^*(z)\Psi_{e1}(z)dz\right|^2. \quad (12)$$

The calculated $S_{e1\text{-}hi}$ values are given in Table II. It is noted that the S(e1-hh1)/S(e1-lh1) ratio is in reasonable agreement with the ratio of the reflection line intensities I(e1-hh1)/I(e1-lh1) as measured for the MDQW's studied here.

C. Photoluminescence spectral shape and hole energy distribution

The additional experimental method that we used in order to examine the calculated dispersion of the top valence subbands was a modulation of the PL spectral shape by varying

TABLE II. Squared overlap integrals and measured relative intensities.

	n_e (cm^{-2})	$S_{e1\text{-}hh1}$	$S_{e1\text{-}lh1}$	$I_{e1\text{-}hh1}/I_{e1\text{-}lh1}$
Two-side	0.9×10^{11}	1.21	0.55	4.5
MDQW	1.8×10^{11}	1.37	0.22	
One-side	0.7×10^{11}	1.18	0.62	1.8
MDQW	2.0×10^{11}	0.71	0.38	

the effective hole temperature T_h. In a previous study,[37] microwave modulation was employed. In the present study, PL excitation was done by illuminating with a Ti: sapphire laser and varying its intensity I_L. We measured the total PL intensity as a function of the exciting laser intensity and found it to be strictly linear over the range of $2<I_L<250$ mW/cm^2 (the only exception is the two-side MDQW with $n_e=1.8\times10^{11}$ cm^{-2} that shows an intensity saturation for $I_L>150$ mW/cm^2 when $E_L=1.584$ eV). This means that nonradiative, saturable processes are virtually ineffective. The experimental PL spectra that are shown in Figs. 2(a) and 2(b) were thus normalized to the integrated intensity. This allows a direct comparison of line shape variation with increasing I_L. It is noted that the high energy cutoff of all PL spectra does not vary with increasing I_L. This means that the effective electron temperature changes only slightly (so that this change cannot be resolved in the PL spectra excited with the highest I_L) and it can be taken to be equal to that of the lattice:[37] $T_e\sim$ T. The photoexcited holes are assumed to relax into the hh1 subband at a faster rate than the radiative recombination rate.[36] According to the PL intensity model [Eq. (11)], the spectral variations that are observed with increasing I_L reflect increasing T_h. By using this model, the calculated curves are obtained (dashed lines in Fig. 2). The good fit of the model to the high energy part of the PL spectra means that the model based on a Boltzmann distribution of the holes in the hh1 subband provides an additional verification of the accuracy of the calculated valence subband dispersion curves. The effective hole temperature dependence on I_L, which is extracted from the PL spectral fittings, is shown in Fig. 8 for the two-side MDQW's.

T_h is found to increase monotonically and it is higher for the same I_L but higher laser excitation energy E_L. It should be noted that in the lower density case, the fit required us to assume an electron density $n_e=0.7\times10^{11}$ cm^{-2}, while the density determined by the freeze-out of the second Landau level is $n_e=0.9\times10^{11}$ cm^{-2}. Also, there is a deviation of the fitted lines from the experimental spectra in the low energy part [Fig. 2(a)]. These findings point at the limitation of the model of a Boltzmann distribution of holes.

We note that the spectra calculated by using Eq. (11) deviate from the corresponding experimental spectra in the low energy range. In particular, the PL intensity decreases monotonically for $E<E_G'$. It is customary to account for this tail by introducing a Gaussian broadening function.[30] Thus, the spectra can be better fitted as shown by the example at the bottom spectrum of Fig. 2(a). We note that the same parameters were used for the fittings, except for T_h that is found to be higher by 1.0 K in the fitting without broadening. Introducing broadening has a negligible effect on the calculated PL spectral shape in the high energy part of the spectrum ($E\sim E_F$). Since this part is most sensitive to the hh1 dispersion and as the origin of the broadening is still unknown, we fitted the PL spectra with Eq. (11), namely, without broadening.

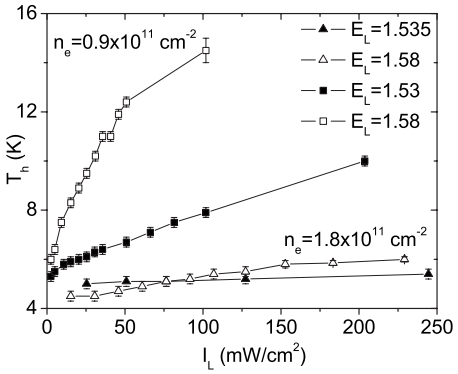

FIG. 8. The effective hole temperature dependence on laser excitation intensity, which is extracted from PL spectral fittings such as those shown in Fig. 2. Square symbols, $n_e=0.9\times10^{11}$ cm^{-2}; triangular symbols, $n_e=1.8\times10^{11}$ cm^{-2}. Two excitation energies were used for each two-side MDQW density, as indicated.

V. SUMMARY

The reflection and PL spectra of several GaAs/Al$_x$Ga$_{1-x}$As MDQW's, which are n doped either on one side of the QW or symmetrically on both its sides, were studied at $T=2$ K. Sharp (but weak) reflection lines are observed and are attributed to e1-hh1 and e1-lh1 interband transitions near k_F of the 2DEG. The energies of these lines were analyzed by calculating the dispersion of the e1, hh1, and lh1 subbands, which include the effect of the Hartree potential of the 2DEG. The analysis of their line shape indicate that there is a weak electron-hole interaction only near k_F. The effect of this interaction is simulated by an enhanced strength of the interband transition dipole in a narrow range around $k_\parallel\sim k_F$. Furthermore, the relative intensity of the reflection lines observed in the one-side MDQW's and in the two-side MDQW's reveals that the intrinsic Fermi edge singularity is mostly determined by the overlap integral of the electron and free hole wave functions at k_F. It should be noted that reflection spectra depend solely on the properties of the photoexcited electron-hole. In the more commonly used method of photoexcitation spectroscopy,[42] relaxation processes are involved and, thus, direct information on the electron-hole pair is more difficult to extract.

The PL spectral shape of both one-side and two-side MDQW's was observed to depend on laser excitation intensity in the same way: the intensity of the higher energy part of the PL band increases with increasing laser excitation intensity. The PL spectra were calculated by using the e1 and hh1 dispersion curves and assuming that the interband transitions conserve the in-plane momentum. The spectral dependence on laser intensity was interpreted by assuming that the

photoexcited holes have a Boltzmann distribution within the hh1 subband, with an effective hole temperature that increases with laser excitation intensity in the range of 4–15 K. The 2DEG heating is negligible and the electron temperature remains unchanged and equal to that of the lattice.

ACKNOWLEDGMENTS

The research at Technion was done in the Barbara and Norman Seiden Center for Advanced Optoelectronics and was supported by the Israel-US Binational Science Foundation (BSF), Jerusalem.

[1] C. Weisbuch and B. Vinter, *Quantum Semiconductor Structures: Fundamentals and Applications* (Academic, New York, 1991), Chap. 3.
[2] S. Schmitt-Rink, D. S. Chemla, and D. A. B. Miller, Adv. Phys. **38**, 89 (1989).
[3] G. D. Sanders and Yia-Chung Chang, Phys. Rev. B **35**, 1300 (1987).
[4] F. G. Pikus, Sov. Phys. Semicond. **26**, 26 (1992).
[5] D. V. Kulakovskii, S. I. Gubarev, and Yu. E. Lozovik, JETP Lett. **74**, 118 (2001).
[6] G. Livescu, D. A. B. Miller, D. S. Chemla, M. Ramaswamy, T. Y. Chang, N. Sauer, A. C. Gossard, and J. H. English, IEEE J. Quantum Electron. **24**, 1677 (1988).
[7] D. Huang, J. Chyi, and H. Morkoc, Phys. Rev. B **42**, 5147 (1990).
[8] R. Harel, E. Cohen, E. Linder, Arza Ron, and L. N. Pfeiffer, Phys. Rev. B **53**, 7868 (1996).
[9] G. Yusa, H. Shtrikman, and I. Bar-Joseph, Phys. Rev. B **62**, 15390 (2000).
[10] M. S. Skolnick, J. M. Rorison, K. J. Nash, D. J. Mowbray, P. R. Tapster, S. J. Bass, and A. D. Pitt, Phys. Rev. Lett. **58**, 2130 (1987).
[11] M. S. Skolnick, D. M. Whittaker, P. E. Simmonds, T. A. Fisher, M. K. Saker, J. M. Rorison, R. S. Smith, P. B. Kirby, and C. R. H. White, Phys. Rev. B **43**, 7354 (1991).
[12] W. Chen, M. Fritze, W. Walecki, A. V. Nurmikko, D. Ackley, J. M. Hong, and L. L. Chang, Phys. Rev. B **45**, 8464 (1992).
[13] G. D. Mahan, Phys. Rev. **153**, 882 (1967).
[14] G. D. Mahan, Phys. Rev. **163**, 612 (1967).
[15] J. W. Wu, Phys. Rev. B **39**, 7992 (1989).
[16] P. Hawrylak, Phys. Rev. B **44**, 3821 (1991).
[17] T. Uenoyama and L. J. Sham, Phys. Rev. Lett. **65**, 1048 (1990).
[18] S. A. Brown, Jeff F. Young, J. A. Brum, P. Hawrylak, and Z. Wasilewski, Phys. Rev. B **54**, R11082 (1996).
[19] J. A. Brum and P. Hawrylak, Comments Condens. Matter Phys. **18**, 135 (1997).
[20] T. Melin and F. Laruelle, Phys. Rev. Lett. **85**, 852 (2000).
[21] J. F. Mueller, Phys. Rev. B **42**, 11189 (1990).
[22] H. Kissel, U. Zeimer, A. Maassdorf, M. Weyers, R. Heitz, D. Bimburg, Y. I. Mazur, G. G. Tarasov, V. P. Kunets, U. Muller, Z. Y. Zhuchenko, and W. T. Masselink, Phys. Rev. B **65**, 235320 (2002).
[23] P. Plochocka-Polack, J. G. Groshaus, M. Rappaport, V. Umansky, Y. Gallais, A. Pinczuk, and I. Bar-Joseph, Phys. Rev. Lett. **98**, 186810 (2007).
[24] L. N. Pfeiffer and K. W. West, Physica E (Amsterdam) **20**, 57 (2003).
[25] S. I. Gubarev, I. V. Kukushkin, S. V. Tovstonog, M. Yu. Akimov, J. Smet, K. von Klitzing, and W. Wegscheider, JETP Lett. **72**, 324 (2000).
[26] B. M. Ashkinadze, V. V. Rudenkov, P. C. M. Christianen, J. C. Maan, and E. Linder, Phys. Status Solidi C **1**, 510 (2004).
[27] T. Ando, A. B. Fowler, and F. Stern, Rev. Mod. Phys. **54**, 437 (1982).
[28] H. Haug and S. W. Koch, *Quantum Theory of the Optical and Electronic Properties of Semiconductors* (World Scientific, New Jersey, 2004), Chap. 5.
[29] A. Kavokin and G. Malpuech, *Cavity Polaritons* (Elsevier, Amsterdam, 2003), Chap. 1.
[30] J. Christen and D. Bimberg, Phys. Rev. B **42**, 7213 (1990).
[31] L. N. Pfeiffer, E. F. Schubert, K. W. West, and C. W. Magee, Appl. Phys. Lett. **58**, 2258 (1991).
[32] L. N. Pfeiffer, K. W. West, J. P. Eisenstein, K. W. Baldwin, and P. Gammel, Appl. Phys. Lett. **61**, 1211 (1992).
[33] S. Adachi, *GaAs and Related Materials: Bulk Semiconducting and Superlattice Properties* (World Scientific, Singapore, 1994), Chap. 9.
[34] J. M. Luttinger, Phys. Rev. **102**, 1030 (1956).
[35] M. Altarelli, U. Ekenberg, and A. Fasolino, Phys. Rev. B **32**, 5138 (1985).
[36] A. Tomita, J. Shah, J. E. Cunningham, S. M. Goodnick, P. Lugli, and S. L. Chuang, Phys. Rev. B **48**, 5708 (1993).
[37] B. M. Ashkinadze, E. Linder, E. Cohen, and L. N. Pfeiffer, Phys. Rev. B **74**, 245310 (2006).
[38] M. Zachau, J. A. Kash, and W. T. Masselink, Phys. Rev. B **44**, 4048 (1991).
[39] U. Ekenberg, L. C. Andreani, and A. Pasquarello, Phys. Rev. B **46**, 2625 (1992).
[40] L. E. Vorobjev, D. V. Donetskii, and L. E. Golub, JETP Lett. **63**, 5138 (1996).
[41] B. V. Shanabrook, O. J. Glembocki, D. A. Broido, and W. I. Wang, Phys. Rev. B **39**, 3411 (1989).
[42] G. Oelgart, M. Proctor, D. Martin, F. Morier-Genaud, F.-K. Reinhart, B. Orschel, L. C. Andreani, and H. Rhan, Phys. Rev. B **49**, 10456 (1994).
[43] L. C. Andreani and A. Pasquarello, Phys. Rev. B **42**, 8928 (1990).
[44] H. Haug and S. W. Koch, *Quantum Theory of the Optical and Electronic Properties of Semiconductors* (World Scientific, New Jersey, 2004), Chap. 4.
[45] Gerald Bastard, *Wave Mechanics Applied to Semiconductor Heterostructures* (Les Editions de Physique, Paris, 1988), Chap. 2.
[46] E. L. Ivchenko, *Optical Spectroscopy of Semiconductor Nanostructures* (Springer-Verlag, Berlin, 2004), Chap. 3.